Nonlinear Analysis and Modeling of Unreinforced Masonry Shear Walls Based on Plastic Damage Model

A.A. Akbarzade M.[1*] and A.A. Tasnimi [2]

1. Ph.D Candidate, Science and Research Branch, Islamic Azad University, Tehran, I.R. Iran,
* Corresponding Author; akbarzadeabbas@ymail.com
2. Professor, Structural Engineering Division, Dept. of Civil and Environmental Engineering, Tarbiat Modares University, Tehran, I.R. Iran

ABSTRACT

Shear behavior and the failure modes of shear stressed masonry walls have been the subject of many investigations. In the present paper, the performance of an interface elasto-plastic constitutive model for the analysis of unreinforced masonry walls by means of micro-finite element modeling is evaluated. The micro-model is utilized to obtain the behavior of unreinforced masonry walls, based on assumption that the masonry bricks, mortar and their interface are three separate elements. In the present modeling, the behavior of bricks and mortar is assumed to comply with the plastic-damage model which is based on multiple damage variables. The behavior of the interface element is assumed to comply with the coulomb friction model having a limit on the critical shear stresses. A nonlinear analysis is performed by the application of explicit formulae in which displacements and rotations between bricks are taken into consideration. To validate the model, experimental results of masonry elements and walls is compared with the results obtained from the numerical analysis. It is concluded that the suggested model is suitable for assessing the behavior of masonry walls under vertical and horizontal loading.

Keywords:
Masonry walls;
Nonlinear analysis;
Isotropic damage model;
Micro-model;
Numerical analysis

1. Introduction

Unreinforced masonry buildings constructed in seismic zones are vulnerable and take a significant risk during an earthquake. In such buildings masonry shear walls are the only structural components which must resist against both gravitational and seismic lateral loadings. Consequently shear behavior and failure modes of masonry walls have been the subject of many investigations. The large number of influencing factors, such as dimensions, material properties and anisotropy of bricks and mortar and joint's width, arrangement of bed as well as head joints and quality of workmanship, make the simulation of masonry buildings extremely difficult. Moreover, an accurate masonry description needs a complete set of experimental data. In many researches, two different approaches based on macro and micro models have been used. The macro-models constitute an effective method to analyze the global response of masonry structures. In such an approach, masonry is regarded as an equivalent material, where mortar and bricks are melted together and appropriate relations are established between averaged masonry strains and averaged masonry stresses. A number of such models have been developed by other authors [1-6]. Among them Lourenco [1] has proposed a nonlinear constitutive model for in-plane loaded walls based on the plasticity theory. Also Massart et al [7] have developed an interesting two-dimensional anisotropic damage model in a "multi-plane" framework.

In micro-model approach, it is possible to characterize mortar, bricks and their interfaces separately, adopting suitable constitutive laws for each component, which take their different mechanical behavior into account [6, 8-12]. The micro-model is probably the best tool available to analyze and

understand the behavior of masonry, particularly concerning its local response but requires an intensive computational effort. To overcome this problem, Tzamtzis [13] and Sutcliffe et al [14] have proposed a simplified micro-modeling procedure which is an intermediate approach, where the properties of mortar and the unit-mortar interface are clamped into a common element, while separate elements are used to represent the brick units.

In this study, a micro-model is used to assess the behavior of masonry shear walls assuming that bricks, mortar and their interface are three separate elements. In this model, the behavior of bricks and mortar is assumed to obey the plastic-damage model developed by Lee and Fenves [15]. This plastic-damage model was developed using the concept of fracture-energy. Two damage variables, one for tensile damage and the other for compressive damage, account for the different damage states. Since mortar and brick similar to concrete, behave differently in tension and compression and also because under the application of reversal loads, their strength in nonlinear region is reduced due to cracking and crushing, therefore this model used for concrete can also be suggested for these materials. Of course in this case, parameters involved should be obtained analytically and experimentally. In this study for bricks and mortar, the yield function proposed by Lubliner et al [16] and modified using multiple damage (or hardening) variables by Lee and Fenves [15] is used. The difference in behavior of the materials used under tension and compression is taken into account in this function. Also the behavior of the interface between mortar and masonry brick is assumed to obey the coulomb friction model having a limit on the critical shear stresses.

A nonlinear analysis is performed by the application of explicit formulae in which displacements and rotations between bricks are taken into consideration. The verification of the analysis was carried out by comparing the numerical results of three experimental tests of masonry units and three masonry shear walls which were experimentally tested under in-plane shear loading and compressive gravitational load. The selected walls are those experimentally studied by Ganz and Thurlimann [17], Raijmakers and Vermeltfoort [18] and Tasnimi [19-20].

2. Theoretical Background

2.1.Brick and Mortar Model

In this model, the behavior of bricks and mortar is assumed to obey the plastic-damage model developed by Lee and Fenves [15]. This plastic damage model has been developed using thermodynamical approach [21-22]. Constitutive relations are derived from thermodynamic potential functions and consequently, they are consistent in the thermodynamic context. In this approach, because well-defined potential functions are required and the associability between state variables and their conjugate forces are preferred, it is difficult to construct the constitutive system based on physical observations, which is more appropriate for modeling quasi-brittle materials such as brick or mortar. For instance, applying the associative plastic flow rule to a model gives a poor result in dilatancy evaluation. Therefore, the constitutive equations for a plastic-damage model are derived in a more direct, but still thermodynamically consistent manner. In this model, two damage variables such as tensile and compressive, account for the different damage states.

Also in this model, difference between the degradation of the elastic stiffness in tension and compression tests is considered. So in either case, the effect is more pronounced as the plastic strain increases.

The yield function proposed by Lubliner et al [16] that was modified using multiple damage (or hardening) variables by Lee and Fenves [15] for bricks and mortar is used. The difference in behavior of the materials used under tension and compression is taken into account in this function. Details of the framework for this plastic-damage model and purposed yield condition are given below.

2.2. Stress-Strain Relations

In the incremental theory of plasticity, the strain tensor ε is decomposed into the elastic part ε^{el} and the plastic part ε^{pl}. The strain rate decomposition is assumed for the rate-independent model as below:

$$\dot{\varepsilon} = \dot{\varepsilon}^{el} + \dot{\varepsilon}^{pl}, \quad \varepsilon^{el} = E^{-1} : \sigma \tag{1}$$

where $\dot{\varepsilon}$ is the total strain rate, $\dot{\varepsilon}^{el}$ and $\dot{\varepsilon}^{pl}$ are the elastic and plastic part of the strain rate respectively, the elastic modulus E is a rank four tensor, and σ is the stress tensor.

The stress-strain relations for bricks and mortar are governed by scalar damaged elasticity:

$$\sigma = K^{el} : (\varepsilon - \varepsilon^{pl}) \quad \text{and} \quad K^{el} = (1-k)K_{\circ}^{el} \tag{2}$$

where $K_{\circ}^{el}$ is the initial or undamaged elastic stiffness of the material, K^{el} is the degraded or damaged elastic stiffness; and k is the scalar stiffness degradation variable, which can take values in the range from zero for undamaged material to one for fully damaged material.

Damage associated with the failure mechanisms of the masonry (cracking and crushing) therefore results in a reduction of the elastic stiffness. Within the context of the scalar-damage theory, the stiffness degradation is isotropic and characterized by a single degradation variable k. Following the usual notions of continuum damage mechanics, the effective stress is defined as:

$$\bar{\sigma} = K_{\circ}^{el} : (\varepsilon - \varepsilon^{pl}) \tag{3}$$

The stress is related to the effective stress through the scalar degradation relation:

$$\sigma = (1-k)\bar{\sigma} \tag{4}$$

For any given cross-section of the material, the factor (1-k) represents the ratio of effective load-carrying area (i.e., the overall area minus the damaged area) to the overall section area. In the absence of damage, k = 0, the effective stress $\bar{\sigma}$ coincides with the stress, σ. When damage occurs, however, the effective stress is more representative than the stress, because it is the effective stress area that is resisting the external loads. It is, therefore, convenient to formulate the plasticity problem in terms of the effective stress.

2.3. Hardening Variables

Generally damaged states in tension and compression are specified independently by two hardening variables which are referred to as equivalent plastic strains in tension ($\tilde{\varepsilon}_t^{pl}$) and equivalent plastic strains in compression ($\tilde{\varepsilon}_c^{pl}$), respectively. It is assumed that the micro-cracking and crushing in the quasi-brittle materials like brick or mortar are represented by increasing values of the hardening variables. These variables control the evolution of the yield surface and the elastic stiffness degradation. They are also referred to the dissipated fracture energy required to generate micro-cracks. Because tensile and compressive damages are quite different in quasi-brittle materials, it is not possible to represent all damage states by a single parameter. To account for the different damage responses of brick or mortar in tension and compression, a multi-hardening (or multi-softening) yield function is used. This function has more than one variable to describe the obtained yield surface. If two state variables σ_t and σ_c represent the uniaxial tensile strength and compressive strength of the material, respectively, the admissible yield function is constrained by the following condition:

$$F(\sigma, \sigma_t, \sigma_c) \le 0 \tag{5}$$

It is assumed that F is an isotropic function in the stress space and a first-degree homogeneous function with respect to all three variables. In the present model, the uniaxial strength function is expressed in terms of two damage parameters k_t and k_c given below:

$$\sigma_t = \sigma_t(k_t) \quad , \quad \sigma_c = \sigma_c(k_c) \tag{6}$$

assuming that both relations in Eq. (6) can be factored into the degradation damage and the effective-stress responses for both tension and compression state yields:

$$\sigma_t = (1-k_t)\bar{\sigma}_t \tag{7}$$

$$\sigma_c = (1-k_c)\bar{\sigma}_c \tag{8}$$

The single degradation damage k can be used to describe both tensile and compressive degradation responses as below:

$$k = k(\tilde{\varepsilon}^{pl}) = 1-(1-k_t)(1-k_c) \tag{9}$$

Note that k in Eq. (9) satisfies the constraint $0 \le k \le 1$ and it is k_t and k_c for uniaxial tensile and compressive case respectively. Since F is a first-degree homogeneous function and the definition of k in Eq. (9) does hold, the yield function can be written as:

$$F(\bar{\sigma}, \tilde{\varepsilon}^{pl}) \le 0 \tag{10}$$

2.4. Damage and Stiffness Degradation

The equations of the hardening variable $\tilde{\varepsilon}_t^{pl}$ and $\tilde{\varepsilon}_c^{pl}$ could be conveniently formulated by considering uniaxial loading conditions that can be extended to multi-axial states.

It is assumed that the uniaxial stress-strain

curves for tension and compression can be converted into stress versus plastic strain curves in the simple form of:

$$\sigma_t = \sigma_t(\tilde{\varepsilon}_t^{pl}, \dot{\tilde{\varepsilon}}_t^{pl}) \tag{11}$$

$$\sigma_c = \sigma_c(\tilde{\varepsilon}_c^{pl}, \dot{\tilde{\varepsilon}}_c^{pl}) \tag{12}$$

The equivalent plastic strains could be evaluated by $\tilde{\varepsilon}_t^{pl} = \int_0^t \dot{\tilde{\varepsilon}}_t^{pl} dt$ and $\tilde{\varepsilon}_c^{pl} = \int_0^t \dot{\tilde{\varepsilon}}_c^{pl} dt$ respectively.

As shown in Figure (1), when the brick or mortar specimen is unloaded from any point on the strain softening branch of the stress-strain curves, the unloading response is observed to be weakened, that is the elastic stiffness of the material appears to be damaged (degraded). The degradation of the elastic stiffness is significantly different between tension and compression tests. So in either case, the effect is more pronounced as the plastic strain increases. The degraded response of masonry is characterized by two independent uniaxial damage variable, k_t and k_c which are assumed to be functions of the equivalent plastic strains,

$$k_t = k_t(\tilde{\varepsilon}_t^{pl}), (0 \le k_t \le 1) \tag{13}$$

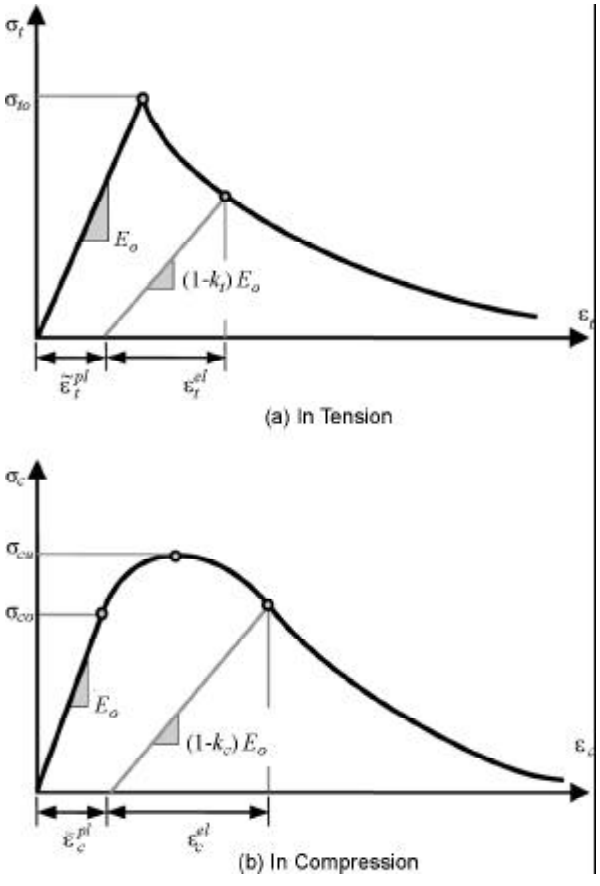

Figure 1. Response of masonry to uniaxial loading.

$$k_c = k_c(\tilde{\varepsilon}_c^{pl}), (0 \le k_c \le 1) \tag{14}$$

The uniaxial degradation variables are increasing functions of the equivalent plastic strains. They can take values ranging from zero to one, for undamaged and fully damaged material respectively. If E_o is the initial (undamaged) elastic modulus of material, the stress-strain relations under uniaxial tension and compression loading are respectively,

$$\sigma_t = (1-k_t)E_o(\varepsilon_t - \tilde{\varepsilon}_t^{pl}) \tag{15}$$

$$\sigma_c = (1-k_c)E_o(\varepsilon_t - \tilde{\varepsilon}_c^{pl}) \tag{16}$$

Under uniaxial loading cracks propagate in a direction transverse to the stress direction. The distribution and propagation of crack, therefore, causes a reduction of the available load-carrying area, which in turn leads to an increase in the effective stress. The effect is less pronounced under compressive loading since cracks run parallel to the loading direction. However, after a significant amount of crushing, the effective load-carrying area is also significantly reduced. The effective uniaxial stresses are given as:

$$\bar{\sigma}_t = \frac{\sigma_t}{(1-k_t)} = E_o(\varepsilon_t - \tilde{\varepsilon}_t^{pl}) \tag{17}$$

$$\bar{\sigma}_c = \frac{\sigma_c}{(1-k_c)} = E_o(\varepsilon_c - \tilde{\varepsilon}_c^{pl}) \tag{18}$$

The effective uniaxial stresses determine the size of the yield (or failure) surface.

2.5. Yield Condition

The plastic damage model uses a yield condition based on the yield function proposed by Lubliner et al [16]. This yield function is modified by Lee and Fenves [15] and hence the yield function takes the following form:

$$F(\bar{\sigma}, \tilde{\varepsilon}^{pl}) = \frac{1}{1-\alpha}(\bar{q} - 3\alpha\bar{p} + \beta(\tilde{\varepsilon}^{pl})\langle\hat{\bar{\sigma}}_{\max}\rangle - \gamma\langle-\hat{\bar{\sigma}}_{\max}\rangle) - \bar{\sigma}_c(\tilde{\varepsilon}^{pl}) \le 0 \tag{19}$$

where γ and α are dimensionless material constants, $\bar{p}$ is the effective hydrostatic pressure, $\bar{q}$ is the Von Mises equivalent effective stress and $\hat{\bar{\sigma}}_{\max}$ (the algebraically maximum eigenvalue of $\bar{\sigma}$) is the maximum principal stress. The function $\beta(\tilde{\varepsilon}^{pl})$ in this equation is given by:

$$\beta(\tilde{\varepsilon}^{pl}) = \frac{\bar{\sigma}_c(\tilde{\varepsilon}_c^{pl})}{\bar{\sigma}_t(\tilde{\varepsilon}_t^{pl})}(1-\alpha) - (1+\alpha) \quad (20)$$

where $\bar{\sigma}_t$ and $\bar{\sigma}_c$ are the effective tensile and compressive stresses, respectively. In biaxial compression, with $\hat{\bar{\sigma}}_{\max} = 0$, Eq. (19) reduces to the well-known Drucker-Prager yield condition. The coefficient α can be determined from the initial equibiaxial and uniaxial compressive yield stress and according to Lee and Fenves [15] is limited to $0 \le \alpha \le 0.5$.

The coefficient γ would be only considered when $\hat{\bar{\sigma}}_{\max} < 0$ for triaxial compression stress state. This coefficient can be determined by comparing the yield conditions along the tensile and compressive meridians. By definition, the tensile meridian (*TM*) is the locus of stress states satisfying the condition $\hat{\bar{\sigma}}_{\max} = \hat{\bar{\sigma}}_1 > \hat{\bar{\sigma}}_2 = \hat{\bar{\sigma}}_3$ and the compressive meridian (*CM*) is the locus of stress states such that $\hat{\bar{\sigma}}_{\max} = \hat{\bar{\sigma}}_1 = \hat{\bar{\sigma}}_2 > \hat{\bar{\sigma}}_3$ where $\hat{\bar{\sigma}}_1, \hat{\bar{\sigma}}_2$ and $\hat{\bar{\sigma}}_3$ are the eigenvalue of the effective stress tensor, it can be easily shown that along the tensile and compressive meridians, the following relations exist:

$$\hat{\bar{\sigma}}_{\max}\big]_{CM} = \frac{1}{3}\bar{q} - \bar{p} \quad (21)$$

$$\hat{\bar{\sigma}}_{\max}\big]_{TM} = \frac{2}{3}\bar{q} - \bar{p} \quad (22)$$

For any given value of the hydrostatic pressure ($\bar{p}$) two cases may be considered:

Case 1) When $\hat{\bar{s}}_{\max} < 0$

In this case the yield conditions along the tensile and compressive meridians are:

For (*TM*); $$\left(\frac{2}{3}\gamma + 1\right)\bar{q} - (\gamma + 3\alpha)\bar{p} = (1-\alpha)\bar{\sigma}_c \quad (23)$$

For (*CM*); $$\left(\frac{1}{3}\gamma + 1\right)\bar{q} - (\gamma + 3\alpha)\bar{p} = (1-\alpha)\bar{\sigma}_c \quad (24)$$

If $\eta_c = \frac{\bar{q}_{TM}}{\bar{q}_{CM}}$ is assumed, then the constant η_c is given by $\eta_c = \frac{\gamma+3}{2\gamma+3}$ and hence $\gamma = \frac{3(1-\eta_c)}{2\eta_c - 1}$.

According to Lubliner et al [16], the constant η_c does not seem to be contradicted by experimental evidence. For quasi-brittle materials like concrete the general value of η_c is $\frac{2}{3}$ from which γ would be 3.

Case 2) When $\hat{\bar{s}}_{\max} > 0$

In this case the yield conditions along the tensile and compressive meridians reduce to:

For (*TM*); $$\left(\frac{1}{3}\beta + 1\right)\bar{q} - (\beta + 3\alpha)\bar{p} = (1-\alpha)\bar{\sigma}_c \quad (25)$$

For (*CM*); $$\left(\frac{2}{3}\beta + 1\right)\bar{q} - (\beta + 3\alpha)\bar{p} = (1-\alpha)\bar{\sigma}_c \quad (26)$$

If $\eta_t = \frac{\bar{q}_{TM}}{\bar{q}_{CM}}$ is assumed, then for any given value of the hydrostatic pressure ($\bar{p}$) and having the condition $\hat{\bar{\sigma}}_{\max} > 0$, then we have $\eta_t = \frac{\beta+3}{2\beta+3}$ and hence $\beta = \frac{3(1-\eta_t)}{2\eta_t - 1}$.

Typical yield surfaces and deviatoric plane for plane stress state are shown in Figures (2a) and (2b), respectively.

2.6. Flow Rule

Plastic flow is governed by a flow potential (*G*) and according to the flow rule we have:

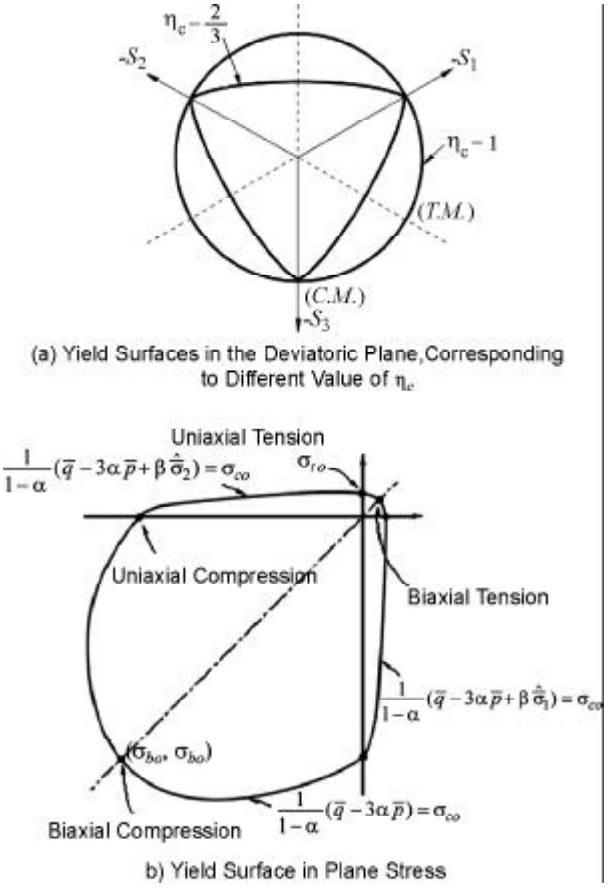

Figure 2. Yield surfaces (a) in the deviatoric plane; (b) in plane stress.

$$\dot{\varepsilon}^{pl} = \dot{\lambda}\frac{\partial G(\bar{\sigma})}{\partial \bar{\sigma}} \tag{27}$$

where $\dot{\lambda}$ is the non-negative plastic multiplier. The plastic potential is the effective stress space. The flow potential (G) chosen for this model is the Drucker-Prager hyperbolic function given below:

$$G = \sqrt{(e\sigma_{to}\tan Y)^2 + \bar{q}^2} - \bar{p}\tan Y \tag{28}$$

where Y is the dilation angle and measured in p-q plane at high pressure; σ_{to} is the uniaxial tensile stress at failure; and e is a parameter referred to as the eccentricity that defines the rate at which the function approaches the asymptote. In summary, the elastic-plastic response of the damaged plasticity model is described in terms of the effective stress and the hardening variables:

$$\begin{aligned} &\bar{\sigma} = K_o^{el} : (\varepsilon - \varepsilon^{pl}) \in \left\{ \bar{\sigma} \,\middle|\, (\bar{\sigma}, \tilde{\varepsilon}^{pl}) \le 0 \right\} \\ &\dot{\tilde{\varepsilon}}^{pl} = h(\bar{\sigma}, \tilde{\varepsilon}^{pl}) . \dot{\varepsilon}^{pl} \\ &\dot{\varepsilon}^{pl} = \dot{\lambda}\frac{\partial G(\bar{\sigma})}{\partial \bar{\sigma}} \end{aligned} \tag{29}$$

Here $\dot{\lambda}$ and F obey the Kuhn-Tucker conditions:

$$\dot{\lambda}F = 0, \quad \dot{\lambda} \ge 0, \quad F \le 0 \tag{30}$$

The stress is calculated in terms of stiffness degradation variable, $k(\bar{\sigma}, \tilde{\varepsilon}^{pl})$ and the effective stress is:

$$\sigma = (1-k)\bar{\sigma} \tag{31}$$

The constitutive relations for the elastic-plastic response, Eq. (29), are decoupled from the stiffness degradation response, Eq. (31), which makes the model attractive for an effective numerical implementation.

2.7. Unit-Mortar Interface Model

The interface between mortar and brick is modeled using coulomb friction model which is based on maximum shear and normal stress applied to the interface. The standard coulomb friction model assumes that two materials sustain the same shear stress and no relative motion occurs if the equivalent frictional stress (τ) is less than the critical stress (τ_{crit}) which is proportional to the contact pressure p, ($\tau = \mu . p + c$). This is also called cohesive limit. Friction coefficient μ and coefficient of cohesion (c) for isotropic materials is supposed to be same in all directions. In three dimensions, two tangential stresses exist at the interface, which are normal to each other i.e. τ_1, τ_2. The equivalent shear stress is therefore given by $\tau_{eq} = \sqrt{\tau_1^2 + \tau_2^2}$ and $\tau_{crit} = \mu . p + c$.

It is possible to put a limit on the critical stress ($\tau_{\max}$):

$$\tau_{crit} = \min(\mu . p + c, \tau_{\max}) \tag{32}$$

If the equivalent stress reaches the critical stress ($\tau_{eq} = \tau_{crit}$), slip can occur. The optional equivalent shear stress limit ($\bar{\tau}_{eq}$) may also be specified so that, regardless of the magnitude of the contact pressure, sliding will occur if the magnitudes of the equivalent shear stress reach this value. This shear stress limit is typically introduced in cases when the contact pressure stress may become very large, causing the Coulomb theory to provide a critical shear stress at the interface that exceeds the yield stress in the material beneath the contact surface. Figure (3) illustrates the slip region for the friction model used for interface element when c = 0.

2.8. Nonlinear Analysis by Applying the Explicit Formulae

The dynamic equation of equilibrium given by Eq. (33) is an ordinary differential equation having

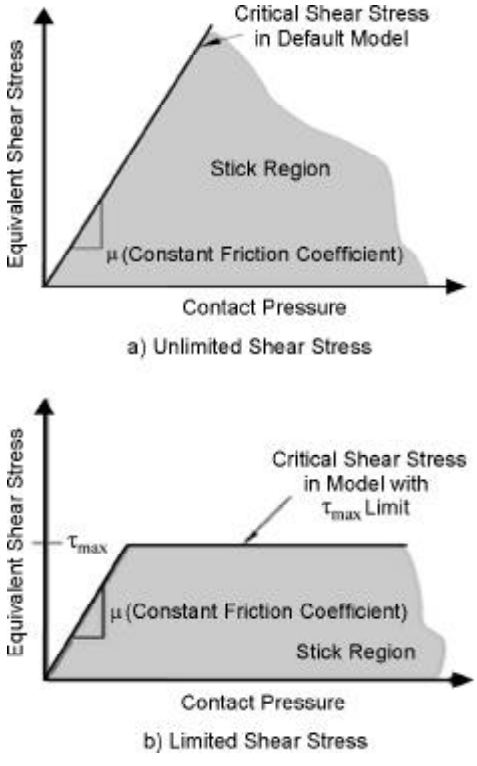

Figure 3. Slip regions for the friction model (c = 0).

constant coefficient.

$$M\ddot{X} + C\dot{X} + KX = R \tag{33}$$

where M, C and K are the mass, damping and stiffness matrices respectively. $X, \dot{X}, \ddot{X}$ and R are the displacement, velocity, acceleration and load vector in time domain respectively.

Many simple finite difference methods can be used to estimate acceleration and velocity with respect to displacement. A method which can be used for solving these problems is the central difference method. In this method it is assumed that:

$$\ddot{X}^{t} = \frac{1}{Dt^2}(X^{t-Dt} - 2X^{t} + X^{t+Dt}) \tag{34}$$

Error in Eq. (34) is of the order (Dt^2). To have the same order of error in velocity formulae, the following equation can be used:

$$\dot{X}^{t} = \frac{1}{2Dt}(X^{t-Dt} + X^{t+Dt}) \tag{35}$$

The response for displacement in the time $(t + Dt)$ can be obtained using the equation;

$$M\ddot{X}^{t} + M\dot{X}^{t} + KX^{t} = R^{t} \tag{36}$$

Substituting in Eq. (36), the following equation is obtained:

$$\left(\frac{1}{Dt^2}M + \frac{1}{2Dt}C\right)X^{t+Dt} = R^{t} - \left(K - \frac{2M}{Dt^2}\right)X^{t} - \left(\frac{1}{Dt^2}M - \frac{1}{2Dt}C\right)X^{t-Dt} \tag{37}$$

Using Eq. (37), the term X^{t+Dt} can be obtained. This integration is an explicit method in which the displacement is independent of acceleration for time (t), and velocity and displacement for the time $(t + Dt)$ can be obtained by using the above equations in time (t). This method is a very simple explicit step-by-step method. However, it is only conditionally stable and will blow up if the time step is not made short enough. It is clear that more effective methods are available, but this method is the simplest procedure and by adopting a shorter time step than others can be used to obtain a satisfactory representation of the dynamic input and response.

In this method in order to satisfy the convergence of analysis, the time increment of Dt should be less than Dt_{cr}:

$$Dt_{cr} = \frac{l_t . l_e}{c} \tag{38}$$

where l_t = 0.7-0.9, l_e is the smallest element dimension, $c = \sqrt{\frac{E}{\rho}}$, E is elastic modulus of materials and ρ is density of material used.

3. Numerical and Experimental Results

To validate the suggested model, during the construction of test specimens, quality control samples were obtained for the mortar, brick and masonry units. The results of numerical analyses are compared with the results of tested masonry units, masonry samples and masonry walls. The control test data contain horizontal or vertical displacements during all states of behavior up to failure. Comparison was deeply carried out between the failure modes and displacement history.

3.1. Prisms Tests

As illustrated in Figure (4), masonry prisms comprising two, three and four bricks were tested to failure and their numerical models were analyzed using material elastic (young modulus and poison ratio) and plastic properties (strength and other plasticity parameters). Some of these material properties were obtained experimentally and some evaluated numerically. The behavior of the interface element is assumed to obey the coulomb friction model having a limit on the critical shear stresses. The detailed description of the analysis method and results interpretation is given in the following.

3.2. Material Properties

3.2.1. Brick

Ten brick samples were loaded in compression according to *ASTM-C*67 to obtain their mechanical properties. From stress-strain curves illustrated in Figure (5a), the average modulus of elasticity of ten bricks (E_b) was evaluated as 135*Mpa*. The average compressive strength of ten brick samples was found to be 9.28*MPa*. By comparing various references, it is supposed that the tensile strength of brick is approximately $\frac{1}{20}$ of its compressive strength [6, 11, 23-25].

3.2.2. Mortar

The mortar mix proportion by volume was 1 part

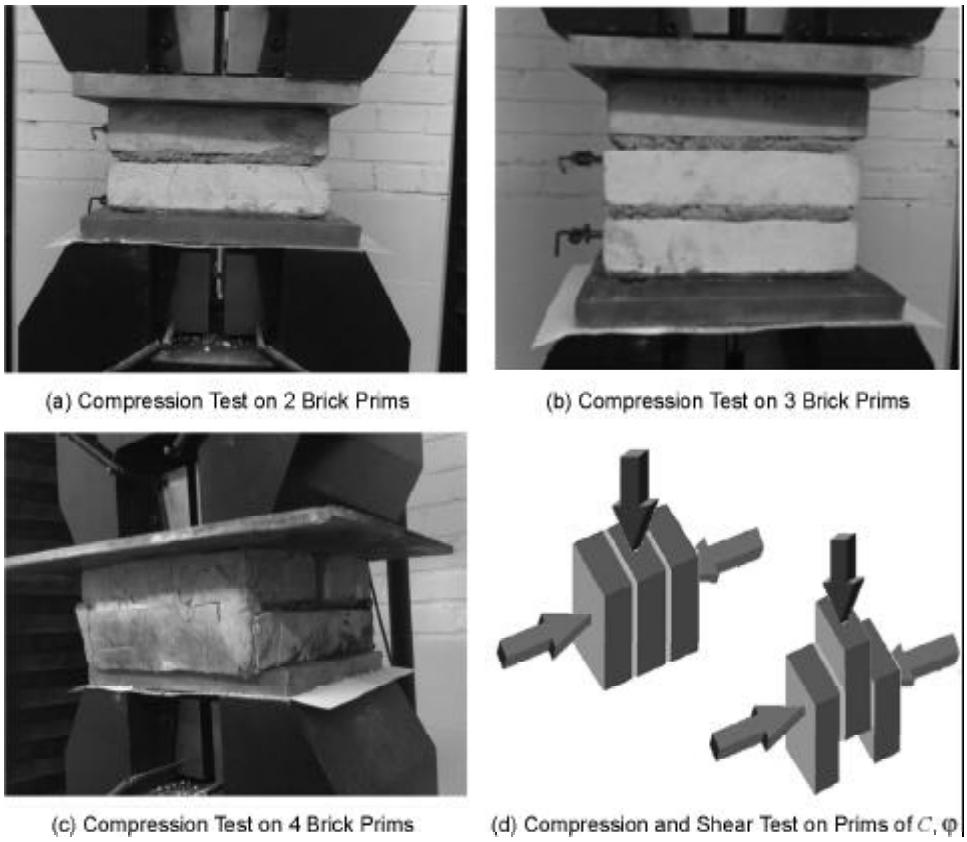

Figure 4. Compression and shear tests of brick prisms.

Portland cement type *I* and 6 parts sand. Ten 50*mm* mortar cube specimens were taken from each mortar mix and tested for compressive strength according to the *ASTM C*-109-1992. The modulus of elasticity of mortar (E_{mo}) was evaluated as 795*Mpa* from the stress-strain curves illustrated in Figure (5b). The average mortar compressive strength (f_{cmo}) was 9.367*MPa*.

Comparing various references, it is supposed that the tensile strength of mortar is approximately of its compressive strength [6, 11, 23-25]. The mortar is stronger and stiffer than brick. Although this contradicts to the most realistic masonry walls in other countries, but the authors have found that this is true for most Iranian made mortar and bricks.

3.2.3. Brick Prisms

Various masonry prisms were built up of clay bricks and 10*mm* thick mortar bed joints. In order to evaluate the compressive strength of masonry units, fifteen 3-course masonry prisms were tested according to *ASTM C*-1314-2000. Using universal testing machine, according to *ASTM-C*952, specimens were subjected to vertical uniformly distributed

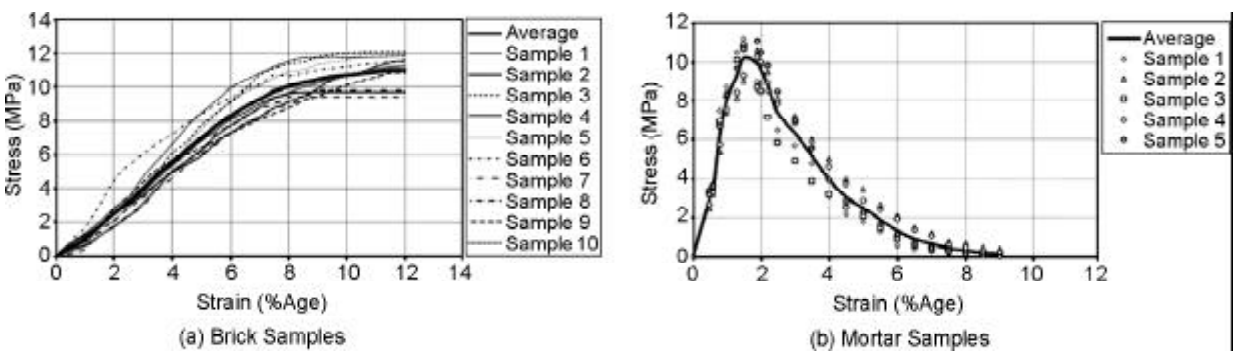

Figure 5. Stress-strain relationship for all bricks and mortars.

load while increasing top controlled displacement until their failure, Figure (4b). The average prism compressive strength (f_{cm}) was 4.26*MPa* and that of modulus of elasticity (E_m) was 207*MPa*.

In this investigation, the average compressive strength of masonry prisms was less than the average compressive strength of the used bricks and mortar. This is due to different material properties that cause vertical splitting of the bricks to occur prior to the crushing of the mortar. It is stated that the higher Poisson's ratio of the mortar results in a tendency for lateral mortar tensile strains to exceed the lateral brick rupture strains [26]. Therefore, the normal compression and lateral biaxial tension in the bricks reduces its crushing strength and induces a tendency for vertical splitting. Masonry prisms failure occurs after the vertical splitting strength of bricks is exceeded which is less than the compressive strength of the bricks and mortar.

The results in Figure (6) show that the highest strength is obtained for the 4 brick masonry units, and the lowest strength occurs in the case with three bricks. This result is reasonable because the similar bricks and mortar are used in these units and the highest strength is obtained for units having lower $\frac{H}{L}$.

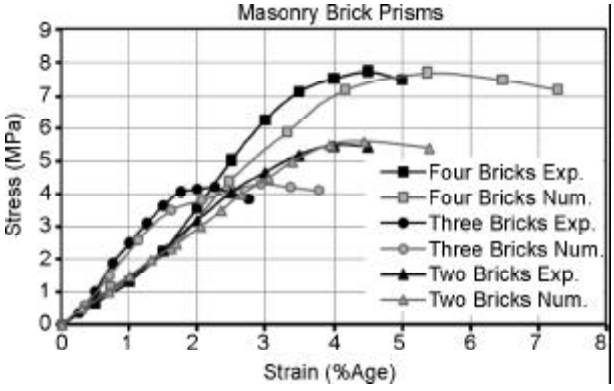

Figure 6. Numerical and experimental stress-strain curves.

As there is no *ASTM* testing procedure given for shear test of masonry samples, the modified triplet specimen for pure shear was used to obtain the mortar shear strength and friction coefficient [27]. This specimen represents the actual shear loading case of masonry walls along the mortar bed joints. The average values of angle of friction (ϕ) and coefficient of cohesion (c) from three prism samples were obtained when they are loaded up to fracture using various constant compression forces together with increasing shear forces, Figure (4d).

3.2.4. Plasticity Parameters

As mentioned, earlier parameters k_c, k_t, α and are η needed for nonlinear state of behavior. However, as the monotonic load was applied (no reversed load) the parameters k_c and k_t are not needed and only α and η are given for the analysis.

As it is difficult to experimentally obtain the plasticity parameters needed for nonlinear analysis, their values were estimated on the basis of excellent agreement between the results of numerical analysis and test results carried out on brick prisms. Of course these parameters are chosen with this view that mortar and bricks behave approximately the same as that of concrete, but are only more ductile. The published Poisson's ratio values for bricks and mortar from other sources are used and not obtained experimentally here [6, 11, 23-25]. Tables (1) and (2) provide the average value of mechanical properties of tested samples and their plasticity parameters.

In order to validate the proposed model, nonlinear numerical analysis was carried out on tested brick prisms whose material properties and plasticity parameters are given in Tables (1) and (2). For numerical analysis of proposed model, rectangular meshes are adopted for the model; and plane stress 4-node bilinear finite elements are used. The bricks and mortar mesh sizes are assumed to be 50*mm* and 10*mm* respectively. With these sizes, the requirement of equation 38 is satisfied. Plastic-damage model was included in the analysis. Using this model and inserting material elastic and plastic properties and brick-mortar interface properties, samples were loaded and analyzed up to failure. The time step was chosen so that the equation 38 is satisfied.

Figure (7) shows the cracking and chipping of bricks in test and numerical analysis. During the experiment, chipping of bricks was observed but it could not be shown in the suggested model. However, the extent of displacement perpendicular to the loading direction is presented in the numerical analyzes which is an indication of bricks chipping.

Also Figure (6) illustrates the comparison between numerical and experimental stress-strain curves of brick prisms with excellent agreement.

Table 1. Mechanical properties (value with * are typical values retrieved from various sources in the literature).

Specimens Tested			Research			
			Present Tests	TASEXP	GANEXP	RAJEXP
Brick		f_{cb} (MPa)	9.28	14.22	9.50	40*
		f_{tb} (MPa)	0.46*	0.7*	0.68	2
		E_b (MPa)	135	8000	5460	16700
Mortar		f_{cmo} (MPa)	9.36	6.23	9.30	10.5
		f_{tmo} (MPa)	0.23*	0.15*	0.28	0.25
		E_{mo} (MPa)	795	1213	2000	15000
Prisms	f_{cbm} (MPa)	2 Bricks	5.54	-	-	-
		3 Bricks	4.26	-	-	-
		4 Bricks	7.22	-	-	-
	f_{tm} (MPa)		-	-	-	-
	E_m (MPa)		207	-	-	-
	Interface Element	f	13	35*	35	36
		c (MPa)	0.3	0.3*	0.3*	0.35

Table 2. Plasticity parameters (value with * are typical values retrieved from various sources in the literature).

Research	Brick			Mortar		
	Poisson Ratio (ν_b)	η_{cb}	α_b	Poisson Ratio (ν_m)	η_{cm}	α_m
PRESENT	0.15*	1.0	0.00	0.2*	0.95	0.045
TASEXP	0.15*	0.85	0.08	0.2*	0.90	0.045
GANEXP	0.18	1.00	0.00	0.18	0.95	0.045
RAJEXP	0.15	0.80	0.08	0.2	0.85	0.045

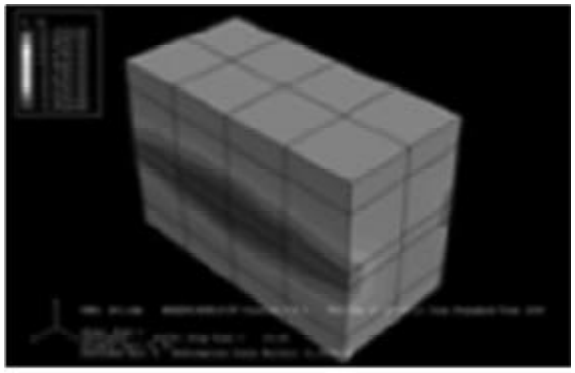

Numerical Cracks and Failure

Experimental Cracks and Failure

Figure 7. Numerical and experimental cracking and chipping of two brick prisms.

3.3. Brick Walls

3.3.1. Wall TASEXP

The numerical analysis of a tested wall (*TASEXP*) carried out by Tasnimi [19] is used to validate this model. The dimensions of this wall were 300*cm* length, 200*cm* height and 20*cm* thickness. This wall was built of solid clay bricks ($212 \times 104 \times 52 mm^3$) and 10*mm* thick mortar made of 1:6 cement to sand ratio by volume. The wall consisted of a masonry panel having lateral concrete flanges at the top to distribute the lateral concentrated loads uniformly. Lateral loads were applied using hydraulic jacks at both sides of the wall. The characteristics of bricks, mortar, and their joints are shown in Table (1). The wall was firstly subjected to a vertical uniformly distributed load $P = 24.53 kN/m$ and then a lateral increasing force was applied on the concrete beam under displacement control. The loading was continued until cracking appeared and up to the threshold of collapse.

For numerical analysis of proposed model, rectangular meshes are adopted for the model and plane stress 4-node bilinear finite elements are used. The behavior of materials used was defined as in the proposed model. As the exact brick-mortar

interface properties of this sample are not given in the relevant reference, the common values are used. The numerical load versus displacement curve for the top row of the wall is compared with the experimental one, see Figure (8). A good correlation and similarity between the experimental results and those of the model is observed.

The collapse mechanism with diagonal cracking through joints and bricks and crushing of the compressed toes are observed in both the model and the experimental results. It should be noted that in the experiment, the applied lateral load was in two directions and the relevant crack patterns were produced in two directions, whereas in numerical analysis the loading is only in one direction.

3.3.2. Wall GANEXP

The numerical analysis of a tested wall *GANEXP* worked out by Ganz and Turlimann [17] is another evidence to validate the proposed model. This wall consisted of a masonry panel having two lateral concrete flanges at the top and bottom. This wall had a total width of 360*cm* and a total height of 200*cm*. The wall was firstly subjected to a vertical uniformly distributed load P =1.91*MPa*, in addition to the self weigh, then a horizontal monotonically increased force was applied on the top flange under displacement control.

Tables (1) and (2) show the characteristics of bricks, mortar, and their joints. For numerical analysis with proposed model, rectangular meshes are adopted for the model. Plane stress 4-node bilinear finite elements are used. The numerical load versus displacement curve is plotted in Figure (9), and compared with the experimental one. A reasonably good agreement is found. As it is evident by the significant development of compressive damage, the failure is dominated by masonry crushing in accordance with the experimental evidence.

3.3.3. Wall RAJEXP

The third tested wall (*RAJEXP*) that was numerically analyzed for the calibration of the proposed model is that tested by Raijmakers and Vermeltfoort [18]. This wall consisted of a pier having a width/height ratio of one ($990 \times 1000\ mm^2$), built up with 18 courses (16 active courses and 2 courses clamped in steel beams) of Joosten solid clay bricks ($204 \times 98 \times 50 mm^3$) and 10*mm* thick mortar (1:2:9, cement, lime and sand by volume). The piers were subjected to a vertical uniformly distributed load P = 1.21*MPa* before a horizontal load was monotonically increased under top displacement control d until failure, see Figure (10). For the numerical analysis, bricks and

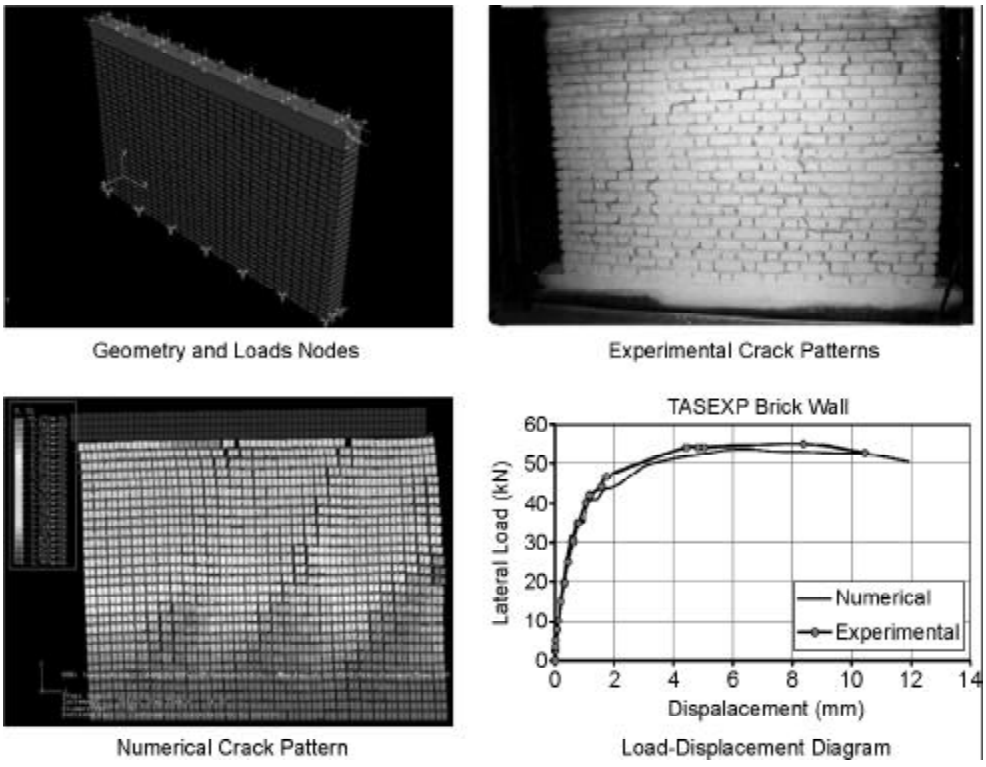

Figure 8. Comparison between numerical and experimental results, Wall TASEXP.

mortar are represented by plane stress continuum elements while interface is modeled by contact elements using Coulomb friction model.

Material properties used in this model are given in Tables (1) and (2). The comparison between numerical and experimental load-displacement

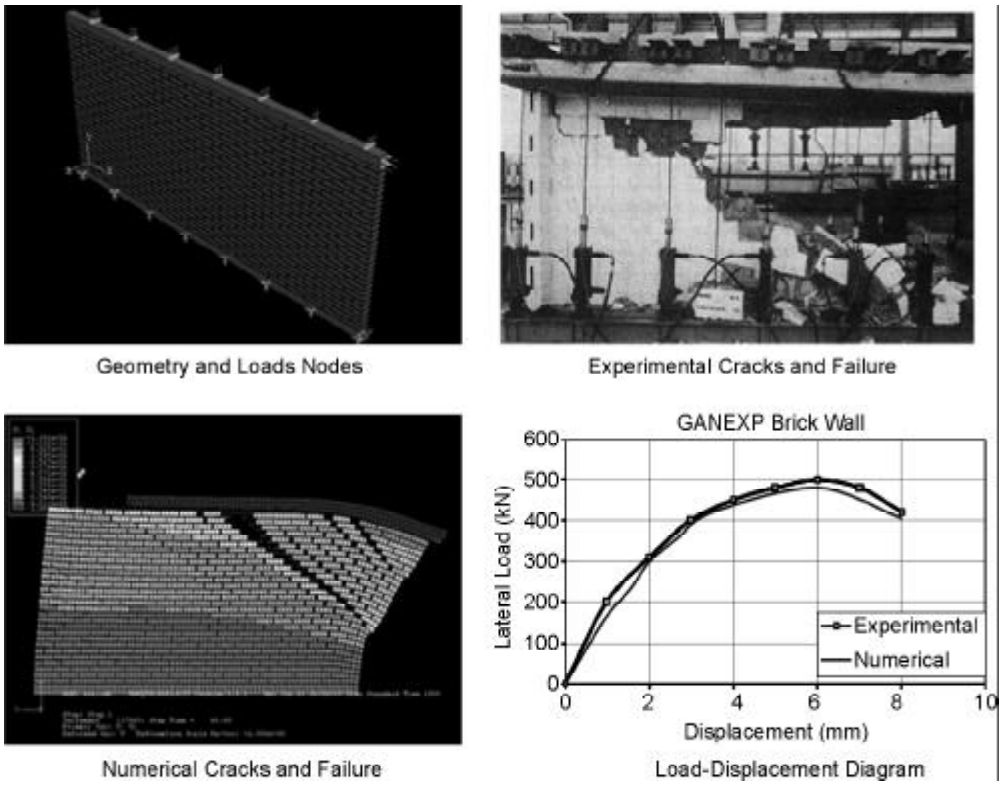

Figure 9. Comparison between numerical and experimental results, Wall GANEXP.

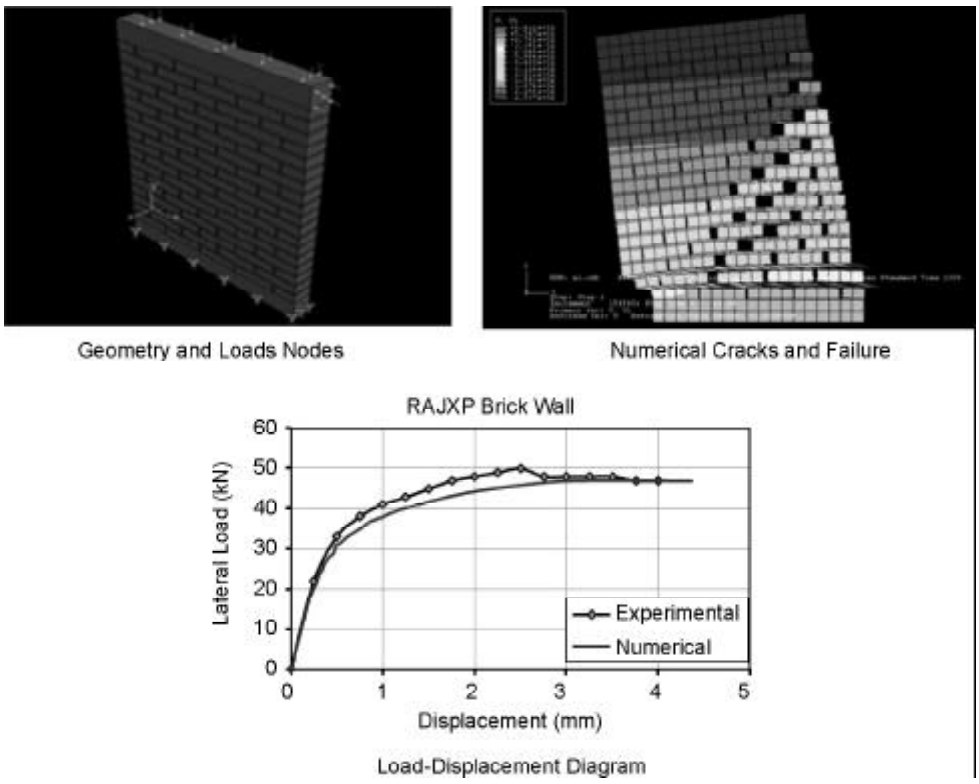

Figure 10. Comparison between numerical and experimental results, Wall RAJEXP.

diagrams is shown in Figure (10). It should be noted that in Figure (10) no picture of the experimental result is included because it was not available in the reference and therefore, the mechanism of failure and horizontal displacement up to failure is presented. It is illustrated that the collapse mechanism is characterized by crushing of the compressed toes and a complete diagonal cracking through joints and bricks in both experimental and numerical results.

4. Conclusions

A micro-finite element model based on the modified yield function utilizing multiple concrete damage variables is proposed for the nonlinear analysis of unreinforced masonry walls. In proposed model, bricks, mortar and their interface assumed to be three separate elements and their behavior obey concrete plastic-damage model developed based on concrete fracture-energy concept. In addition, independent tensile and compressive behaviors for all materials are considered. The behavior of the interface element is assumed to obey the coulomb friction model having a limit on the critical shear stresses. However the research reported in this article leads to the following conclusions:

- The proposed model is suitable for linear and nonlinear analysis of unreinforced masonry walls with no limitation on the consideration of various variables such as geometrical dimension and material properties.
- Based on micro consideration in the analysis the localized cracking and failure could be predicted accurately.
- The tensile and compressive behavior of brick and mortar and that of interface element would be easily considered in all state of behavior up to collapse.
- The proposed model is capable to recognize the failure mode of the *URM* walls.
- The plasticity parameters of the used material could not be easily evaluated which may cause some error on the wall capacity.

References

1. Lourenco, P.B. (1996). "*Interface Model Applied to Fractures*", Delft University Press, Delft, The Netherlands.

2. Callerio, A. and Papa, E. (1998). "In: Pande Middleton and Kralj, Editor. An Elastic-Plastic Model with Damage for Cyclic Analysis of Masonry Panels", Computer Methods in Structural Masonry-4, E&FN Spon, London.

3. Zhuge, Y., Thambiratnam, D., Corderoy, J. et al (1998). "Non-Linear Dynamic Analysis of Un-Reinforced Masonry", *Journal Structural Engineering, ASCE,* **124**(3), 270-277.

4. Syrmakezis, C.A. and Asteris, P.G. (2001). "Masonry Failure Criterion under Biaxial Stress State", *Journal Material Civil Engineering*, **13**(1), 58-64.

5. Andreaus, U. (1996). "Failure Criteria for Masonry Panels under In-Plane Loading", *J. Structural Engineering, ASCE*, **122**(1).

6. Berto, L., Saetta, A., Scotta,R., and Vitaliani, R. (2004). "Shear Behaviour of Masonry Panel: Parametric FE Analyses", *International J. of Solids and Structures*, **41**, 4383-4405.

7. Massart, T.J., Bouillard, Ph., Geers, M.G.D., and Peerlings, R.H.J. (2001). "A 2D Anisotropic Damage Model for Masonry Walls", *Proceedings of V European Conf. on Computational Mechanics*, Cracow, Poland.

8. Page, A.W. (1978). "Finite Element Model for Masonry", *Journal Structure Division, ASCE*, **104**(ST8), 1267-1285.

9. Ali, S.S. and Page, A.W. (1988). "Finite Element Model for Masonry Subjected to Concentrated Loads", *Journal Structural Engineering, ASCE,* **114**(8), 1761-1784.

10. Lofti, H.R. and Shing, B.P. (1994). "Interface Model Applied to Fracture of Masonry Structure", *Journal Structural Engineering, ASCE,* **120**(1), 63-80.

11. Lurenco, P.B. and Jan, G.R. (1997). "Multisurface Interface Model for Analysis of Masonry Structures", *J. of Engineering Mechanics*, **123**(7), 660-668.

12. Zucchini, A. and Lourenco, P.B.A. (2002). "Micro-Mechanical for the Homogenization of Masonry", *Int. Journal Solids Structure*, **39**,

3233-3255.

13. Tzamtzis, A.D. (1994). "Dynamic Finite Element Analysis of Complex Discontinuous and Jointed Structural Systems Using Interface Elements", Ph.D. Thesis, Department of Civil Engineering, QMWC, University of London.

14. Sutcliffe, D.J., Yu, H.S., and Page, A.W. (2001). "Lower Bound Limit Analysis of Unreinforced Masonry Walls", *Comput. Structure*, **79**, 1295-1312.

15. Lee, J., Fenves, G.L. (1998). Member, ASCE. "Plastic-Damage Model for Cyclic Loading of Concrete Structures", *Journal of Engineering Mechanics*, **124**(8), 892-900.

16. Lubliner, J., Oliver, J., Oller, S., and Onate, E. (1989). "A Plastic-Damage Model for Concrete", *Int. Journal Solids and Structure*, **25**(3), 299-326.

17. Ganz, H.R. and Thurlimann, B. (1984). "Tests on Masonry Walls under Normal and Shear Loading", Report No. 7502-4, ETH Zurich Institute of Structural Engineering, Zurich (in German).

18. Raijmakers, T.M.J. and Vermeltfoort, A.T. (1992). Deformation Controlled Meso Shear Tests on Masonry Piers", Rep. B-92-1156, TNOBOUW/TU Eindhoren, Building and Construction Research, Eindhoren, The Netherlands (in Dutch).

19. Tasnimi, A.A. (2004). "Behavior of Brick Walls Recommended by Standard 2800", Building and Housing Research Center (BHRC), PN. R-404, Tehran, Iran.

20. Tasnimi, A.A. (2005). "Behavior of Confined and Unconfined Masonry Brick Buildings", Natural Disaster Research Institute of Iran, Tehran, Iran.

21. Ju, J.W. (1989). "On Energy-Based Coupled Elastoplastic Damage Theories: Constitutive Modeling and Computational Aspect", *Journal Solids and Struct.*, **25**(7), 803-833.

22. Hansen, N.R. and Schreyer, H.L. (1994). "A Thermodynamically Consistent Framework for Theories of Elastoplasticity Coupled with Damage", *Int. J. Solids and Struct.*, **31**(3), 359-389.

23. Massart, T.J, Peerlings, R.H.J, and Geers, M.G.D. (2004). "Mesoscopic Modeling of Failure and Damage-Induced Anisotropy in Brick Masonry", *European J. of Mechanics A/ Solids*, **23**, 719-735.

24. Gabor, A., Ferrier, E., Jacquelin, E., Hamelin, P. (2005). "Analysis and Modeling of the In-Plane Shear Behavior of Hollow Brick Masonry Panels", Construction and Building Materials.

25. Massart, T.J., Peerlings, R.H.J., Geers, M.G.D., Gottcheiner, S. (2005). "Mesoscopic Modeling of Failure in Brick Masonry Accounting for Three-Dimensional Effect", *Engineering Fracture Mechanics*, **72**, 1238-1253.

26. Paulay, T. and Priestley, M.J.N. (1992). "*Seismic Design of Reinforced Concrete and Masonry Buildings*", John Wiley & Sons, Inc., New York, USA.

27. Harris, H.G. and Sabnis, G.M. (1999). "*Structural Modeling and Experimental Technique*", CRC Press, New York, USA.

Notations

c : Coefficient of cohesion
C : Damping matrix
e : Eccentricity parameter (defines the rate at which the function approaches the asymptote)
E : Elastic modulus (a rank four tensor)
E_o : Initial (undamaged) elastic modulus (a rank four tensor)
F : Isotopic function in the stress space / first-degree homogeneous function
f'_m : Uniaxial compressive strength normal to bed joint
G : Flow potential
k : Scalar stiffness degradation variable
K : Stiffness matrix
K^{el} : Degraded or damaged elastic stiffness
K_o^{el} : Initial or undamaged elastic stiffness
l_e : The smallest element dimension
M : Mass matrix
p : Normal stresses at interface (contact pressure)

$\bar{p}$: Effective hydrostatic pressure
$\bar{q}$: Von Missies equivalent effective stress
R: Load vector in time domain
$\bar{s}$: Deviatoric part of the effective stress tensor
X: Displacement in time domain
$\dot{X}$: Velocity in time domain
$\ddot{X}$: Acceleration in time domain
α: Material parameters, determine the shape of the Hill yield surface
β: Material parameters, determine the shape of the Hill yield surface
γ: Material parameters, determine the shape of the Hill yield surface
Dt: Time increment
Dt_{cr}: Critical time increment
ε: Strain tensor
ε^{e}: Elastic part of strain tensor
ε^{p}: Plastic part of strain tensor
$\dot{\varepsilon}$: Total strain rate
$\dot{\varepsilon}^{el}$: Elastic part of strain rate
$\dot{\varepsilon}^{pl}$: Plastic part of strain rate
$\tilde{\varepsilon}_{t}^{pl}$: Equivalent plastic strains in tension (Hardening variable)
$\tilde{\varepsilon}_{c}^{pl}$: Equivalent plastic strains in compression (Hardening variable)
η: Material parameters, determine the shape of the Hill yield surface
$\dot{\lambda}$: Non-negative plastic multiplier
μ: Coefficient of friction defined as a function of the contact pressure
v_b: Brick poisson ratio
v_m: Mortar poisson ratio
ρ: Density of material
σ: Stress tensor
$\bar{\sigma}$: Effective stress
σ_y: Von Misses yield stress of the material
σ_{to}: Uniaxial tensile stress at failure
$\hat{\bar{\sigma}}_{to}$: Algebraically maximum eigenvalue of $\bar{\sigma}$
τ: Tangential stresses exist at the interface
τ_{crit}: The critical shear stress
$\tau_{\max}$: The maximum shear stress
ϕ: Angle of friction
ψ: Dilation angle